Neural network potential for CrCoNi system (Version 1)

Jun-Ping Du[a,b,*], Shigenobu Ogata[b,a,*]

[a] *Center for Elements Strategy Initiative for Structural Materials, Kyoto University, Kyoto 606-8501, Japan.*
[b] *Department of Mechanical Science and Bioengineering, Osaka University, Osaka 560-8531, Japan.*

1. Architecture of NNP

We adopted the high-dimensional neural network potential (NNP) developed by Behler and Parrinello [1] to construct the NNP for CrCoNi medium entropy alloy. The energy of system in the HDNNP is expressed as

$$E_{tot} = \sum E_n, \tag{1}$$

where E_n is the atomic energy. The atomic energy is calculated as

$$E_n = f_1^3\left\{b_1^3 + \sum_k a_{k1}^{23} * f_k^2\left[b_k^2 + \sum_j a_{jk}^{12} * f_j^1(b_j^1 + \sum_i a_{ij}^{01} * G_i)\right]\right\} \tag{2}$$

where $f_1^3(x) = x$, $f_k^2(x) = \ln(1+\mathrm{e}^x)$ and $f_j^1(x) = \ln(1+\mathrm{e}^x)$ are the activation functions, b_1^3, b_k^2, b_j^1, a_{k1}^{23}, a_{jk}^{12} and a_{ij}^{01} are the weight parameters of NNP, G_i is the symmetry functions characterized the local chemical environments of the atom. The following two types of symmetry functions were adopted for atom i and its all neighbors j and k,

$$G_i^2 = \sum_j e^{-\eta R_{ij}^2} f_c(R_{ij}) \tag{3}$$

and

$$G_i^3 = 2^{1-\xi} \sum_{j\neq i} \sum_{k\neq i,j} \left[(1+\lambda\cos\theta_{ijk})^{\xi} e^{-\eta(R_{ij}^2+R_{ik}^2+R_{jk}^2)} f_c(R_{ij}) f_c(R_{ik}) f_c(R_{jk})\right], \tag{4}$$

where η, ξ, λ are pre-defined parameters before training the NNP. The $f_c(R_{ij})$ is a cutoff function defined as

$$f_c(R_{ij}) = \begin{cases} \tanh^3(1 - R_{ij}/R_c), & R_{ij} \leq R_c \\ 0, & R_{ij} > R_c \end{cases} \tag{5}$$

and the cutoff distance $R_c = 6$ Å. For each element, we adopted 87 symmetry functions in the input layer. Between the input layer and the output layer, there are 2 hidden layers and each hidden layer contains 12 nodes.

*Email: jpdu@tsme.me.es.osaka-u.ac.jp (J.P.D.), ogata@me.es.osaka-u.ac.jp (S.O.)

2. DFT datasets

The DFT datasets for training NNP should sample the configurational space of atoms as much as possible to ensure the wide applicability of the potential. The high entropy alloys (HEAs) are characterized by its configurational complexity. Even we only consider the first-nearest neighboring interaction, there are 3^{13}=1,594,323 possible atomic configurations for a ternary system including both the equivalent and the inequivalent configurations. To sample the inequivalent configurations systematically, we used the *mmaps* code of the ATAT package [2] to generate a set of inequivalent atomic configurations with up to 7 atoms and 3 types of elements in a primitive cell. The atoms arrangements were set in FCC, BCC and HCP structures in the primitive cells, respectively. The possible composition of the ternary alloys in the primitive cells ($Cr_xCo_yNi_z$) was constrained by $0 \leq x \leq 1$, $0 \leq y \leq 1$, $0 \leq z \leq 1$, and $x+y+z=1$, so that our NNP potential can be used not only in equiatomic HEA, but also in the monoatomic or binary atomic solid solution, e.g. in the condition of phase separation of HEA. These primitive cells constructed by *mmaps* were relaxed with respects to cell volume, shape and atomic positions using VASP [3–5]. To describe the elastic properties of HEA, the relaxed primitive cell consisting of $1 \sim 6$ atoms were applied to three types of deformation on the cell lattice, that is $(\delta, \delta, \delta, 0, 0, 0)$, $(1+\delta', 1-\delta', 0, 0, 0, 0)$ and $(0, 0, 0, \delta', 0, 0)$, where $0.9 \leq \delta \leq 1.5$ and $0 \leq \delta' \leq 0.05$ with an interval of 0.01. The static calculation results of the deformed primitive cells were included in the DFT datasets. The vacancy is one of the elementary lattice defects, which is related to the diffusion of metal atoms in the HEAs and the formation of SRO. Thus, we also prepared the primitive cells of FCC-CrCoNi with vacancy using *mmaps*, where vacancy concentration is equal or less than 0.25 and the models were relaxed with respects to cell volume, shape and atom positions using VASP. To include the atomic configurations of vacancy diffusion, 24 diffusion pathways in an equiatomic $(3 \times 3 \times 3)a_0$ FCC-CrCoNi model and each pathway consisting of 5 images obtained by NEB calculations [6] with VASP were included in the DFT datasets. In order to include the information of SRO in the training data, we adopted an equiatomic $(3 \times 3 \times 3)a_0$ FCC–CrCoNi model, where $a_0 = 3.52$ Å, and performed 1,000 times of swapping of two atoms with different types of elements successively. After every swapping, the static energies were calculated using VASP and also included in the DFT datasets.

Except for the above mentioned configurations where atoms are located at or nearby their equilibrium positions, we also performed first-principles molecular dynamic (FPMD) simulations under constant volume and constant temperature using the following models to sample the configurational space deviated from their equilibrium positions. (1) Based on a $(2 \times 2 \times 2)a_0$ FCC supercell with 31 atom and one vacancy, where $a_0 = 3.5$ Å, we generated 21 supercell models by randomly setting the type of the atoms as Co, Cr or Ni with equal probability. The temperature of the FPMD simulations ranges from 300 K to 1500 K with an interval of 300 K. (2) Accompanying with the crystalline structure, the models of equiatomic HEA with liquid state are also included in the DFT datasets. Ten models with 108 atoms randomly located within in 10.6 Å×10.6 Å×10.6 Å supercells were designed

and the FPMD simulations were performed at the temperature of 2000 K. (3) The equiatomic HEA with (100), (110), (111) and (112) surfaces were designed using slab models and FPMD simulation were performed at 300 K and 600 K. (4) The cluster structures with different sizes include models from dimmer to 55-atom clusters and the FPMD simulation were performed at 300 K.

The exchange correlation between electrons in the spin-polarized VASP calculations was treated with the generalized gradient approximation [7] in the PBE form and the energy cutoff was $1.3 \times E_{\max}$, where $E_{\max}$ is the largest value of the default maximum energy cutoff of the plane-wave basis of Cr, Co and Ni.

3. Construction of NNP

The total DFT datasets consists of 149,928 structures (3,436,433 atoms). The energies of the structures were used to train the NNP with the n2p2 code [8]. In the n2p2 code, the DFT datasets are divided into two part: training data and testing data. 90% of the energies of structures were randomly selected as the training data and the remanding data were used as the testing data. The comparison between the energies from the DFT and the NNP are shown in Fig. 1. The root of mean squared error of the training data and the testing data are 13 meV/atom and 15 meV/atom, respectively.

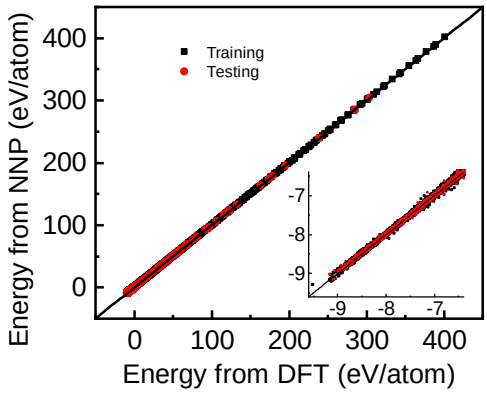

Figure 1: Energies of training set from the DFT calculations and the NNP. The solid lines indicate the points where the DFT results equals to the NNP results.

References

[1] Jörg Behler and Michele Parrinello. Generalized neural-network representation of high-dimensional potential-energy surfaces. *Physical review letters*, 98(14):146401, 2007.

[2] Axel Van De Walle. Multicomponent multisublattice alloys, nonconfigurational entropy and other additions to the alloy theoretic automated toolkit. *Calphad*, 33(2):266–278, 2009.

[3] Georg Kresse and Jürgen Hafner. Ab initio molecular dynamics for liquid metals. *Physical Review B*, 47(1):558, 1993.

[4] Georg Kresse and Jürgen Hafner. Ab initio molecular-dynamics simulation of the liquid-metal–amorphous-semiconductor transition in germanium. *Physical Review B*, 49(20):14251, 1994.

[5] Georg Kresse and Jürgen Furthmüller. Efficient iterative schemes for ab initio total-energy calculations using a plane-wave basis set. *Physical review B*, 54(16):11169, 1996.

[6] Graeme Henkelman, Blas P Uberuaga, and Hannes Jónsson. A climbing image nudged elastic band method for finding saddle points and minimum energy paths. *The Journal of chemical physics*, 113(22):9901–9904, 2000.

[7] John P Perdew, Kieron Burke, and Matthias Ernzerhof. Generalized gradient approximation made simple. *Physical review letters*, 77(18):3865, 1996.

[8] Andreas Singraber, Tobias Morawietz, Jörg Behler, and Christoph Dellago. Parallel multistream training of high-dimensional neural network potentials. *Journal of chemical theory and computation*, 15(5):3075–3092, 2019.